ceramics

Review

The Modified Random Network (MRN) Model within the Configuron Percolation Theory (CPT) of Glass Transition

Michael I. Ojovan [1,2]

1   Department of Materials, Imperial College London, South Kensington Campus, Exhibition Road, London SW7 2AZ, UK; m.ojovan@imperial.ac.uk
2   Department of Radiochemistry, Moscow State University Named after M.V. Lomonosov, Leninskie Gory 1, Bd.3, 119991 Moscow, Russia

Abstract: A brief overview is presented of the modified random network (MRN) model in glass science emphasizing the practical outcome of its use. Then, the configuron percolation theory (CPT) of glass–liquid transition is concisely outlined, emphasizing the role of the actual percolation thresholds observed in a complex system. The MRN model is shown as an important tool enabling to understand within CPT the reduced percolation threshold in complex oxide systems.

check for **updates**

1. Introduction

The modified random network (MRN) model of glasses proposed first by Greaves [1–4] has been nowadays confirmed by many observations in experiment and modeling. The molecular structure of a glass controls the glass properties—for example, the chemical durability—by establishing the distribution of ion exchange sites, hydrolysis sites, and the access of water to those sites. Therefore, it is imperative to investigate the molecular structure of glass evidencing the details of medium-range order (MRO) of glasses. The MRN model involves two interlacing disordered sub-lattices (regions), one of which contains the well-polymerized silica skeleton (covalent network), while the other is depolymerized and comprises of large concentrations of network modifiers such as alkalis. The first model of glass structure was the continuous random network (CRN) model, which became a classical method of thinking on structures of glasses and melts presenting the molecular structure of oxide glass formers as a topologically disordered network of corner-sharing tetrahedra forming rings and cages [5]. Experiments indicated that the CRN model cannot describe the structure of melts and glasses containing modifying metal cations.

The MRN model accounts that the metal cations such as Na^+, K^+, Ca^{2+}, Mg^{2+} break the inter-tetrahedral bonds and segregate into clusters, which gradually grow so that at higher concentrations, they eventually become continuous channels once their concentration reaches the percolation threshold [1–4,6]. Figure 1 is schematically representing the MRN model of an alkali silicate glass structure [7].

The MRN model allows Al-free silicate glasses and melts to be well described, whereas aluminosilicate glasses are different. The Al^{3+} in silicates enters mostly in tetrahedral coordination in the form of negatively charged AlO_4^- with apical oxygen atoms presenting electrical charge deficits. As a result, the metal cations that are present in the melt compensate for this electrical charge deficit as they do in the crystalline state. In most aluminosilicate glasses for practical uses, the concentration of metal cations provides almost exactly the charge compensation of the AlO_4^- present, this effect being used to bind radioactive hazardous nuclides in nuclear waste immobilization [8]. These effects are accounted by the compensated CRN (CCRN) model [9] by locating compensating metallic ions in the vicinity of AlO_4^-. Thus, the CCRN is essentially a variant of MRN which properly accounts for

the aluminosilicate case and specifies that cations occupy in well-defined sites in silicate systems. The MRN involving cations clustering is confirmed by X-ray and neutron spectroscopy measurements [1–4,6,9], laser mass spectroscopy data [7], Raman and Nuclear Magnetic Resonance measurements [10], Molecular Dynamics (MD) simulations [6,10], and modification of melts viscosity, demonstrating that metal ions nano-segregate into percolation channels, making this a universal phenomenon of oxide glasses and melts [10]. MD simulations of alkali-silicate glasses strongly support the MRN model of glass: (a) confirming the existence of silica-rich regions and the clustering of sodium ions in these glasses [11], and (b) evidencing decoupling the structure into alkali-associated and alkali-migration-blocking parts [12]. It has been found that the X-ray irradiation damages to some extent in the Na-containing silicate glasses slightly increased the total bridging oxygen atoms content of the glass at the expense of NBO, thus increasing the polymerization of the glass, while polymerization may cause channels to become segmented into unconnected pockets where ionic species are concentrated [13].
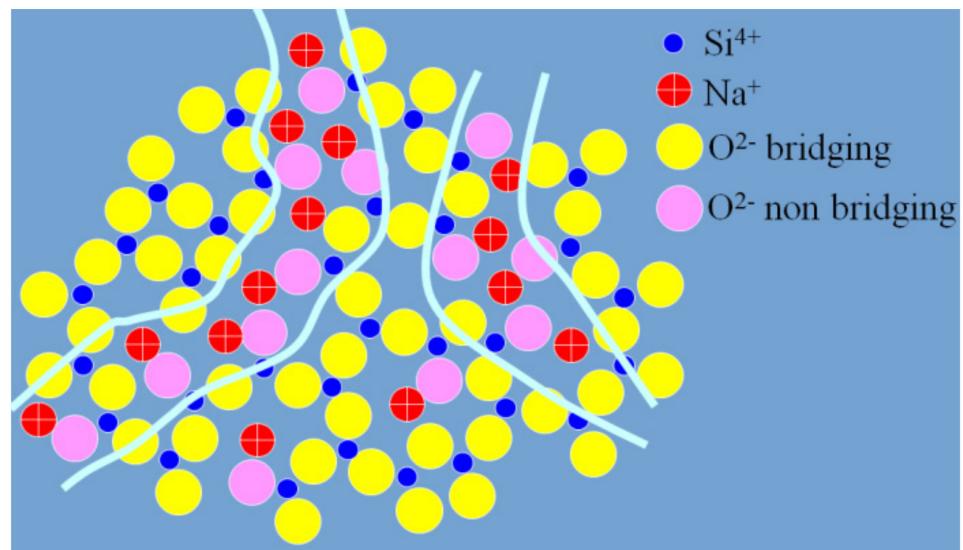

Figure 1. Schematic of modified random network (MRN) model of sodium–silicate glass with percolation ionic channels formed by alkali cations associated with non-bridging oxygens (NBOs). Ionic radii are as follows: $r(Si^{4+})$ = 54 pm, $r(Na^+)$ = 116 pm, $r(O^{2-})$ = 126 pm. The regions comprised of large concentrations of network modifiers so that alkalis form ionic percolating channels at higher concentrations—in silicate glasses typically at <67 mol.% of silica, whereas at higher content of silica, these regions are isolated from each other by the silica skeleton (network regions). The SiO_4 tetrahedra define the network regions, while non-bridging oxygen (NBO) atoms define depolymerized regions that can form percolation channels. The percolation ionic channels are defined by the NBO atoms at the edges of the highly ordered network regions, which ionically bond to the alkali, alkaline earths, or other modifier species in a glass.

Thus, the MRN model has two interlacing topologically disordered sub-lattices: the network sub-lattice and another lattice with regions comprised of large concentrations of network modifiers in form of clusters that form percolation channels. It has been found that for small length scales, the percolation channels have fractal geometry with Hausdorff–Bezicovich dimensionality (D) in the range from 1.5 to 2.0, whereas on macroscopic scales, the D rapidly increases to 3. The fractal structural feature of oxide glasses explains the well-known mixed alkali effects in glasses as caused by the blocking by immobile unlike cations. It has been revealed that the blocking effect is highly effective namely due to low dimensionality of pathways on local length scales (D is less than 3) [14]. A mixed alkali effect (conductivity) is caused by the blocking by immobile unlike cations, and the blocking effect is highly effective due to low dimensionality pathways on local length scales. It has been also revealed that the developments in alkali cluster formation in compensated

aluminosilicate melts are responsible for the anomalous substantial rise in melt viscosity when one metal ion is replaced by a larger one [10].

The cationic percolation channels can be visualized as they act as ion-exchange paths for elements that are less well bonded in glasses. Indeed, cations being bound to the NBO result in the fact that the ion exchange occurs along percolation channels that exist in the glass structure. The percolation channels have been experimentally observed at the glass–gel interface when the leached layer was removed [15]. Ion exchange occurs along percolation channels that exist in glass, and the dissolution appears to follow percolation channels. It has been revealed that on fracturing, the alkali-silicate glasses form fresh surfaces that are enriched in alkalis and so supporting the MRN model of glasses (Figure 2).
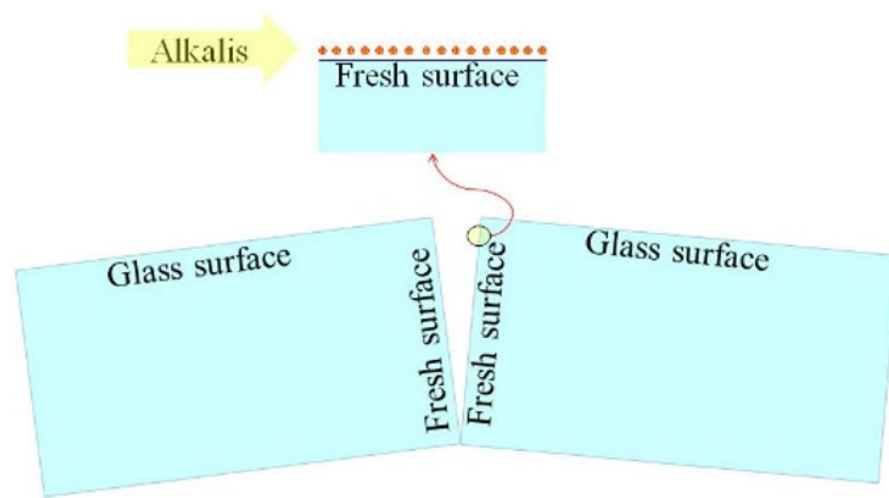

Figure 2. Crushing of complex oxide glass samples creates new surfaces enriched in alkali.

Mass spectrometric analysis of newly formed surface on breaking sodium borosilicate glasses revealed that newly formed surfaces are significantly enriched with sodium. They have also a slightly higher content of boron and are depleted in Mg, Ca, Al, Ti, and Mo compared with the initial glass surface [7].

2. CPT of Glass Transition

The configuron percolation theory (CPT) of glass transition [16–19] specifies that although glasses are isotropic and homogeneous macroscopically, the structure of glasses comprises the following features: (i) at the atomic size, the short-range order (SRO) with molecular-type units such as tetrahedral structures in silicates, (ii) at a larger size range, the medium-range order (MRO) extends from second and third-neighbor environments to percolating and fractal structures, and (iii) at macroscopic sizes, the disordered state (DS) is homogeneous and isotropic.

The SRO in oxide glasses and melts is represented by polyhedral structural units such as tetrahedral and octahedral structural units with typical sizes about 1.6–3 Å. The SRO structural groups in commercial glasses are usually tetrahedral Si, B, Al, Fe, and P surrounded by four oxygen atoms (tetrahedral coordination) or B surrounded by three oxygen atoms (trigonal coordination). The tetrahedra and trigonal species in glass link to each other via bridging oxygen (BO) bonds. The remaining non-bridging oxygen atoms (NBOs) effectively carry a negative charge and ionically bond positively charged cations such as Na^+ or Ca^{2+}. The regions are comprised of large concentrations of network modifiers so that alkalis form ionic percolating channels at higher concentrations—in silicate glasses typically at about 67 mol% of silica, whereas at higher content of silica, these regions are isolated from each other by the silica skeleton (network regions). NBO are located at the interface between the ionic channels and the covalent network and BO are located within the network regions [15,20]. The SiO_4 tetrahedra define the network regions,

while NBO atoms define depolymerized regions that can form percolation channels. The percolation ionic channels are defined by the NBO atoms at the edges of the highly ordered network regions, which ionically bond to the alkali, alkaline earths, or other modifier species in a glass (Figure 1). The MRN model is indeed associated with the structural heterogeneity in glass. For example, Moesgaard et al. [21] provided the direct, strong NMR evidence for the structure heterogeneity at medium-range scale in silicate glasses, i.e., the existence of less polymerized Ca-Si-O domains (corresponding to the percolation floppy domain in MRN) and fully polymerized AlO_4-SiO_4 domains (rigid domains). Moreover, the fragile region and strong region coexist in glass, as reported in [22].

The transition of a glass to a liquid (the glass transition) on increase of temperature of glasses demonstrates clear thermodynamic origins [23–27], although the transformation is kinetically controlled so that the temperature of glass transition (T_g) depends weakly (logarithmically) on the heating rate [28,29]. Figure 3 shows schematically the most prominent changes that occur at glass to liquid transitions.

Glass-forming liquids vitrify on cooling down at the T_g, so the amorphous materials become typically brittle, although the drastic changes of materials properties at the glass transition make the structural changes of a vitrifying liquid extremely difficult to reveal directly. This became possible on utilizing sophisticated atomic force microscopy (AFM) techniques [33], analysis of fifth-order susceptibility [34], and analysis of X-ray pair distribution function [29], whereas the theoretical treatment in terms of structural changes is mainly dealt in works that consider the association of atomic and molecular species forming glasses i.e., clustering behavior [16–19,35–37]. Structural changes become most evident on analyzing the bond system of materials as first proposed by Angel-Rao [38]. The bond lattice model which was proposed by Angel and Rao aimed to replace the set of atoms by a congruent structure of weakly interacting bonds—the congruent bond lattice (CBL). In the CBL, the system of weakly interacting chemical bonds denoted congruently replaces the initial system of strongly interacting ions such as Si^{4+} and O^{2-} in SiO_2. Thus, the system of N strongly interacting particles (Si^{4+} and O^{2-} for silica glass) is replaced by a system of N' = NZ weakly almost non-interacting bonds where Z is the coordination number (Z = 4 for silica glass). In the case when atoms are not bonded via bridging atoms (such as oxygen in silica), which is typical for metallic glasses—for example, for glassy Ni, then N' = NZ/2.

We have used the set theory, which is a branch of mathematical logic that studies abstract sets as collections of objects [39]. In our case, we applied the set theory to the set of chemical bonds which can be either intact or broken due to thermal fluctuations. In such a way, we are dealing with a typical two-level system that is well developed theoretically as a tool to describe amorphous materials and the glass transition [40,41]. Focusing on just broken bonds termed configurons reveals that at absolute zero T = 0, there are no broken bonds in the glass, whereas at finite temperatures, broken bonds are formed by thermal fluctuations. The configurons at low temperatures are point-like objects and do not form extended associations (clusters). The situation changes drastically when a macroscopic cluster made of broken bonds (configurons) is formed for the first time, which penetrates the whole bulk of an amorphous material. That occurs at the temperature T_g found from the condition of formation of the percolation cluster made of broken bonds.

The system of bonds of CBL is a set of contacting although practically not interacting objects which we do represent as equivalent spheres [16–19]. If a certain fraction p of spheres is conducting and the rest are non-conducting, then what is the value of critical fraction p_c at which long-range conduction first occurs? Conducting spheres in our case are equivalent to broken bonds (configurons) whereas intact bonds are equivalent to non-conducting spheres. We assume that the radii of broken bonds in first approximation are equal to radii of unbroken bonds, although generically, an account should be paid on increase of radii on bond breakage. An important development in the understanding of percolation thresholds in disordered (randomly distributed) systems was the introduction of the critical volume fraction (θ_c) by Scher and Zallen [42]. For regular lattices of any objects

such as spheres with uniform nearest-neighbor bond lengths of unity, they considered placing spheres of unit diameter at each vertex with a fraction of space occupied by spheres giving the filling fraction f. Multiplying this quantity by the site percolation threshold p_c yields $\theta_c = p_c f$. For the three-dimensional systems that were studied, it was found that the θ_c falls in a narrow range of 0.144–0.163. Generically, it is considered that the invariant occurs for the critical volume fraction $\theta_c = 0.15 \pm 0.01$, and this fraction is termed the Sher–Zallen invariant [42,43]. It is important to note that in contrast to the free-volume model of liquid–glass transition [44], the CPT operates with the volume of configurons, which is a characteristic of chemical bonds only and does not represent the overall free (non-occupied) volume of the material [16–19]. Melting of an amorphous material i.e., the transition from glassy to molten state occurs when broken bonds form a percolation cluster that penetrates the entire bulk of the material and so changes macroscopically the rigidity of system. The concentration of configurons can be calculated as a function of temperature using an equivalent two-level system that consists of unbroken (ground level) and broken (excited level) bonds [16,17]. The fraction of configurons $\phi(T) = C_d/C_0$ where C_d is the concentration of broken bonds and C_0 is the total concentration of bonds in the CBL as a function of temperature:

$$\phi(T) = \frac{\exp(-G_d/RT)}{1 + \exp(-G_d/RT)}, \tag{1}$$

where G_d is the configuron formation Gibbs free energy $G_d = H_d - TS_d$, H_d is the enthalpy, S_d is the entropy of formation of configurons, and R = 8.314 J/K mol is the gas constant. The condition when a fraction content of broken bonds $\phi(T) = C_d/C_0$ equalizes the percolation threshold ϕ_c determines the first time a percolation cluster made of broken bonds—configurons—is formed. Thus, it gives the temperature of glass transition as:

$$T_g = \frac{H_d}{S_d + R\ln[(1 - \phi_c)/\phi_c]}. \tag{2}$$

Thus, T_g is dependent on quasi-equilibrium thermodynamic parameters of bonds that are related to the enthalpy (H_d) and entropy (S_d) of formation of bonds (configurons) at given conditions which do not necessarily need to be equilibrium conditions but rather adiabatically follow the temperature of the system. At temperatures above T_g, the material contains configurons at concentrations that exceed the threshold ϕ_c; therefore, the broken bonds form a percolation cluster with fractal geometry changing the state of material from solid-like (glass) to liquid-like (melt). Equation (2) provides exact data for T_gs of SiO$_2$ and GeO$_2$ glasses when the threshold $\phi_c = \theta_c = 0.15 \pm 0.01$ [16,17], whereas more complex substances acquire smaller thresholds $\phi_c \ll 0.15$ [18,19]. The glass-transition temperature although being a thermodynamic parameter is kinetically controlled and depends on the thermal schedule used for several reasons: (i) a part of the material is inevitably crystallized during thermal treatment, (ii) configurons need a certain time to relax to their equilibrium sizes, and (iii) the enthalpy of configuron formation depends on the overall state of amorphous material including its quenched density.

The glass–liquid transition in the CPT shows typical features of second-order phase transformations so that derivatives parameters such as the thermal expansion coefficient and specific heat capacity diverge at T_g. Namely, the isobaric heat capacity of glasses $C_p(T)$ on the scanup of temperature at T close to T_g has the following temperature dependence [16–19]:

$$C_p(T) = \frac{C_0}{|T - T_g|^{1-\beta}}, \tag{3}$$

where the critical index β for the three-dimensional space is $\beta = 0.41$ [42,43]. This is due to the formation of a percolation cluster made of configurons. The vitrification of melts is not accompanied by configuron clusters formation; thus, there cannot be discontinuities in the temperature dependence of C_p on temperature downscan and just a gradual decrease of it on cooling down of melts.
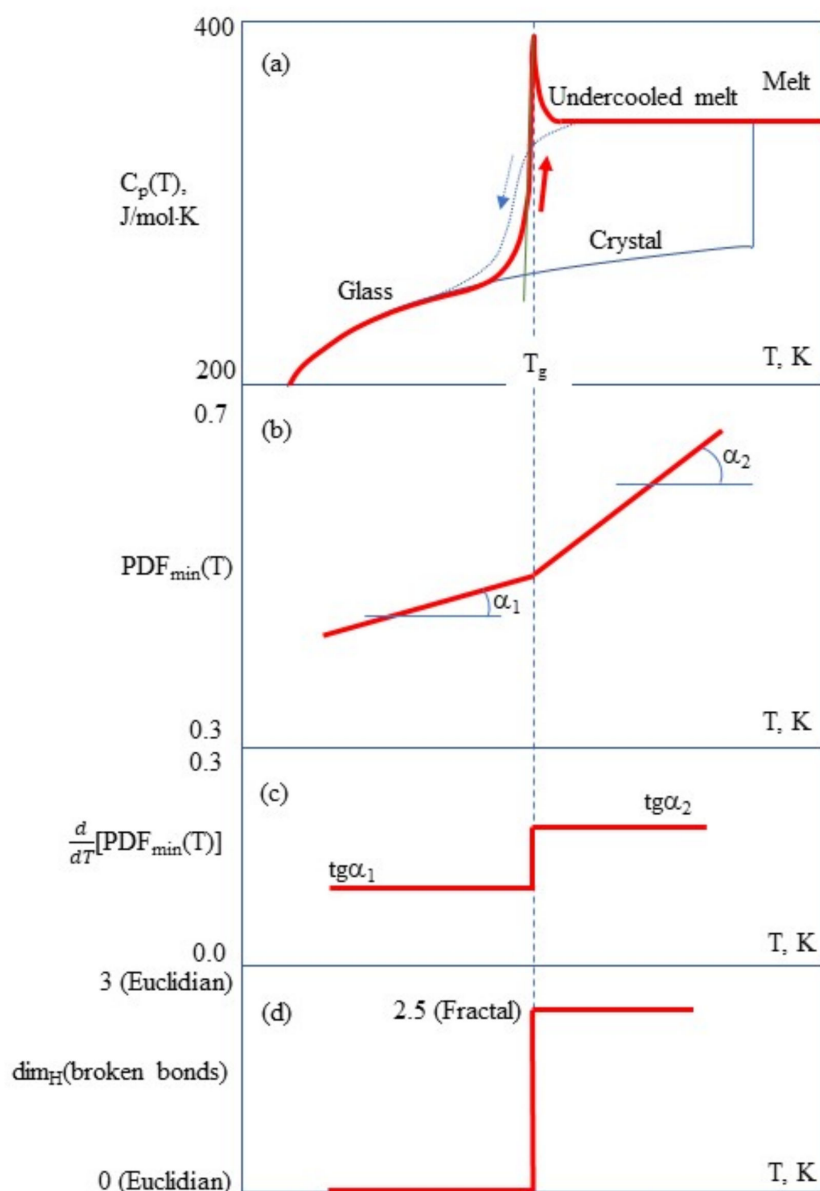
Figure 3. The main characteristics of glass–liquid transition that demonstrate the thermodynamic origin and structural changes behind transformation. (**a**) The temperature (T) dependences of the isobaric heat capacity (C_p) by differential scanning calorimetry (DSC) during the heating of a glass at a typical rate of 10 K/min. The glass−liquid transition during upscan is always featured by a C_p jump, whereas the vitrification (liquid−glass transition) on cooling during downscan is reflected by a gradual C_p drop [30]. (**b**) The temperature dependence of the first sharp diffraction minimum (FSDM) value of pair-distribution function (PDF_{min}) on the scattering of incident neutron or X-rays indicating that at the T_g there is a substantial change of slope due to structural changes at the glass transition [31]. (**c**) The temperature dependence of the first temperature differential of FSDM value $d(PDF_{min})/dT$ indicating that at the T_g, there is a stepwise change of slope due to structural changes at the glass transition [31]. (**d**) The temperature dependence of the Hausdorff–Besicovitch dimension $D = dim_H$(broken bonds) of the set of broken chemical bonds at the glass transition changes suddenly as change the material properties. The set of broken bonds termed configurons has $D = 0$ below the T_g, and $D = 2.55 \pm 0.05$ above it [32].

The Hausdorff–Besicovitch dimension D of the set of broken bonds at the glass transition changes suddenly as change the material properties (Figure 2). The Hausdorff–

Besicovitch dimension in our case is equivalent to the Minkowski–Bouligand dimension based on box-counting, which is defined as the limit:

$$D = \lim_{\varepsilon \to a} \frac{logN(\varepsilon)}{\log(1/\varepsilon)},$$ (4)

where $N(\varepsilon)$ is the number of boxes of side length ε required to cover the set of broken bonds (configurons). When $N(\varepsilon)$ grows proportionally to $1/\varepsilon^D$ as ε tends to zero, then we conclude that the set has the Hausdorff–Besicovitch dimension D. In the counting procedure, we start with macroscopic large lengths, diminishing them step by step to microscopic scales (Figure 4).
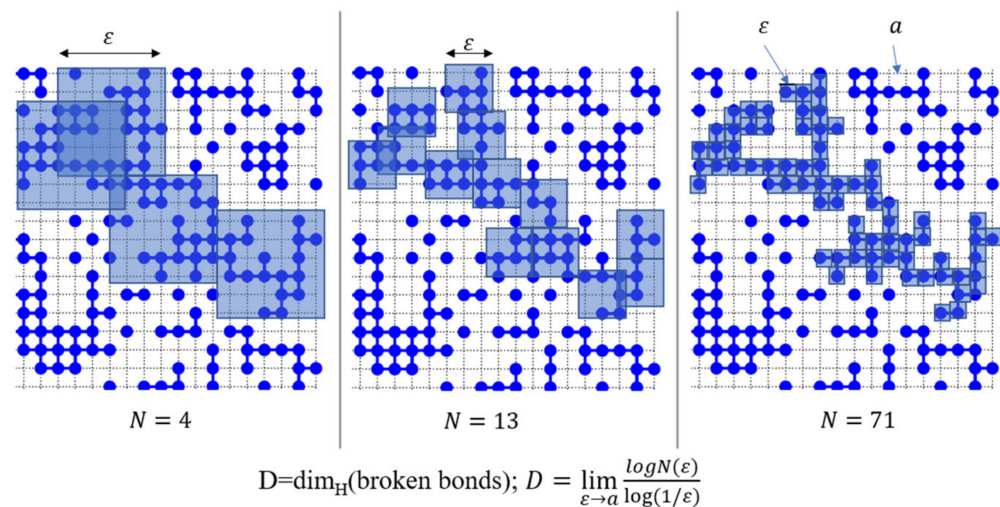

$$D=\text{dim}_\text{H}(\text{broken bonds}); \quad D = \lim_{\varepsilon \to a} \frac{logN(\varepsilon)}{\log(1/\varepsilon)}$$

Figure 4. Schematic of finding Hausdorff–Besicovitch dimension *D* of the percolation cluster made of a set of connecting sites representing configurons on a planar square lattice of bonds. Blue dots are configurons, and the percolation is evidenced by the connecting pathway from the left to right sites of the square. The theoretical result for two-dimensional square lattices is *D* = 1.896, and the percolation threshold p_c = 0.59, meaning that 59% of bonds shall be broken in order for percolation via broken bonds to occur [43].

In mathematics, the limit in Equation (4) is formally drawn to zero, whereas we account that the minimal length in physical systems is equal to the bond size, which is half of the interatomic distance. The percolation cluster made of configurons is a typical macroscopic fractal. The set of broken bonds has *D* = 0 below the T_g, and *D* = 2.55 ± 0.05 above it [32].

The bonds set with bonds intact is characterized by Hausdorff–Besicovitch dimension *D* = 3. This conforms to the known result that the Euclidian space R^n has a Hausdorff–Besicovitch dimension *D* = n. Moreover, whether the distribution of bonds is ordered or disordered is unimportant; in both cases, the three-dimensional bond structures have the same *D* = 3. Thus, in both cases of glasses and crystals, we have the same Hausdorff–Besicovitch dimension *D* of the bonds set and therefore the same mechanical behavior. Two types of topological disorder characterized by different symmetries can be revealed in an amorphous material as a function of temperature based on the analysis of the set of broken bonds (Figure 3d). (i) The first is the 0-dimensional set, which occurs at low temperatures when the configurons are uniformly distributed within the bond structure with no macroscopic clusters are formed. The bonds can be characterized as point-like defects of CBL. (ii) The second is the *D* = 2.55 ± 0.05-dimensional fractal set, which occurs at the glass transition temperature when the percolation cluster made of broken bonds is formed with preferential pathways for configurons which are mobile and can jump from one to another CBL site.

The characteristic linear scale that describes the branch sizes of dynamic clusters formed by configurons near T_g is the correlation length $\xi(T)$. It gives the linear dimension above which the material is fully homogeneous so that a material with sizes larger than $\xi(T)$ has on average uniformly distributed configurons. However, at sizes equal or smaller than $\xi(T)$, the material is dynamically inhomogeneous and is characterized by the fractal geometry [43,45] because of the formation of the percolation cluster, which is fractal by its structure. It means that the glass loses at glass–liquid transition the invariance for the Euclidian space isometries such as translation and rotation on length scales smaller than $\xi(T)$. The liquid near the glass transition is dynamically inhomogeneous on length scales smaller than $\xi(T)$ and remains unchanged for a fractal space group of isometries. At temperatures far from the T_g, the correlation length is small, whereas at temperatures approaching T_g, it diverges:

$$\xi(T) = \frac{\xi_0}{|\phi(T) - \phi_c|^\nu},$$ (5)

where ξ_0 is a certain elementary length of the order of the bond length, and the critical exponent ν in the three-dimensional space is $\nu = 0.88$ [43]. As a result of that, if the sample sizes L are smaller than $\xi(T)$, the amorphous material is dynamically inhomogeneous and has a fractal geometry. Finite size effects in the glass transition are described as a drift to lower values of T_g when sample sizes L decrease [16,17]:

$$T_g(L) = T_g(bulk)\left[1 - \left(\frac{\alpha_{cpt}}{L}\right)^\delta\right],$$ (6)

where $T_g(bulk)$ is the glass transition temperature for large-size samples when $L >> \xi(T)$, $\alpha_{cpt} = \xi_0[7.843RT_g(bulk)/H_d]^\nu$, $\delta = 1/\nu$, and $\nu = 0.88$ is the critical exponent. This equation conforms well with experiments and theory [46] and are also applicable to thin polymeric films [47].

The heat capacity per mole of configurons involved in the percolation cluster near the T_g was found as [16,17]:

$$C_{p,conf} = R\left(\frac{H_d}{RT}\right)^2 \phi(T)[1 - \phi(T)]\left(1 + \frac{\beta P_0 \Delta H T_1^{1-\beta}}{H_d|T - T_g|^{(1-\beta)}}\right),$$ (7)

where $T_1 = RT_g^2/\phi_c(1 - \phi_c)H_d$, P_0 is a numerical coefficient close to one e.g., when $\phi_c = \theta_c = 0.15 \pm 0.01$, we have $P_0 = 1.0695$, and $\Delta H << H_d$ is the enthalpy of configurons in the percolation cluster. At $T \to T_g$ Equation (7) reduces to (3), demonstrating second-order phase transformation-like behavior with heat capacity diverging near the transformation temperature T_g.

Recently, liquid glasses were discovered experimentally in suspensions of ellipsoidal colloids that similarly to liquid crystals demonstrate glass-like properties before being melted [48]. It is well known from earlier investigations that emulsions exhibit fractal structures at small sizes [49]; however, structural imaging at high concentrations has been limited to systems composed of spherical colloids. The authors of [48] revealed that suspensions of ellipsoidal colloids form an unexpected state of matter, a liquid glass in which rotations are frozen while translations remain fluid. The nematic precursors were characteristic structural elements of this state, and the mutual obstruction of these ramified clusters prevented liquid crystalline order. Thus, we can generalize the state of matter schematic proposed in [50] as a function of connectivity and ordering (Figure 5).

The discovery of liquid glasses and liquid crystals suggest that the dimensionality of structures forming a material are important for the analysis of phase transformation. Table 1 shows data from percolation theory [43,45] on the critical most important parameters at glass–liquid transition.
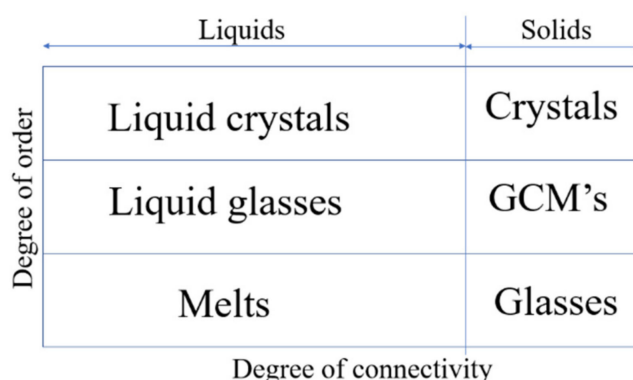
Figure 5. Schematic of phase state as function of ordering and connectivity between building blocks (molecules) of materials. GCMs are glass composite materials containing both crystalline and vitreous phases.

Table 1. Critical parameters for 2 and 3-dimensional structures (sets).

Dimension of System, d	3 (Bulky)	2 (Planar)
Scher–Zallen critical density (invariant), θ_c	0.15 ± 0.01	$0.44 + 0.02$
β	0.41	0.14
ν	0.88	1.33
Fractal dimension $D = d - \beta/\nu$	2.55 ± 0.05	1.896

Indeed, from Equation (2), we can see that because the critical density θ_c in the 2-dimensional systems is much larger compared with 3-dimentional structures, their T_g values are higher; i.e., the melting (glass–liquid transition) for planar-type liquid glasses will occur much later that for 3-dimensional glasses. Thus, first, 3-dimentional glasses will melt, and then some remnant 2-dimensional glasses will melt if any.

Finally, we note that the CPT provides the bases for the viscosity of amorphous materials being described by the Sheffield model of viscosity [51,52]. The two-exponential Sheffield equation of viscosity:

$$\eta(T) = A \cdot T \cdot exp(H_m/RT)] \cdot [1 + C \cdot exp(H_d/RT)], \tag{8}$$

where A, H_m, C, and H_d are material specific constants, gives a correct description of viscosity with two exact Arrhenius-type asymptotes both for melts much above the T_g, and glasses much below the T_g. Within the low temperature, the activation energy of viscosity is high $Q_H = H_d + H_m$, whereas at high temperatures, the activation energy is low $Q_L = H_m$. The Arrhenius behavior of viscosity at low and high temperatures is a known experimental result tested for glass forming liquids and ancient glasses and denying low-temperature diverging predictions of other models [53–55].

3. The MRN in the CPT

Broadbent and Hammersley have first introduced the percolation model on the example of a porous stone immersed in water where they were looking on the probability that the center of the stone is wetted [56]. The flow of water in the porous stone was named percolation because the fluid flow into the maze resembles coffee flowing through the grounds in a percolator [45,57]. Applications of percolation theory include many useful practical cases such as the spread of forest fires, oil and gas exploration, electrical properties of disordered media, gelation, polymerization, etc. The general formulation of percolation theory considers elementary geometrical objects such as spheres, squares, or sticks placed at random in a d-dimensional lattice or continuum [43,45]. These objects have a well-defined connectivity radius λ_0 so that two objects are considered communicating if the distance between them is less than λ_0. A cluster is simply a group made of communicating objects.

Cluster sizes can change, and therefore, an important question is when the clusters become infinite. This is controlled by the density of objects n_0 in the space of dimensionality d or by the dimensionless density (filing factor), which is defined as $\eta = n_0 \cdot (\lambda_0)^d$. The percolation threshold η_c is defined as such a density $\eta = \eta_c$ when the clusters made of communicating objects span the space. Although ordered lattice formulation of the percolation theory is very convenient, most natural systems are disordered rather than have a perfect lattice structure. It was found that independently of lattice type for each dimension d, the percolation occurs at an invariant critical fraction of space occupied by spheres of the bond length diameter positioned in the occupied sites of the lattice θ_c [42]. The critical space occupational probability is $\theta_c = 0.44 \pm 0.02$ for d = 2 and $\theta_c = 0.15 \pm 0.01$ for d = 3 (Table 1). However, this is the case of simplest systems of monodisperse objects. Meanwhile, local heterogeneity can have a major effect on percolation threshold. For example, anisotropic communicating objects such as rods can more easily connect to each other and percolate at much lower volume fractions (space occupational probability) $\phi_c \ll \theta_c$ [45]. In contrast to that, the polydisperse spheres have a higher threshold volume fraction for percolation that can reach units, which means that they can practically fully fill the space without forming percolating clusters [58]. Equation (2) with $\phi_c = \theta_c$ for complex glass-forming liquids overestimates the T_g values by about 20% [18]. It shows that complex materials made of more complex molecular units are characterized by significantly smaller percolation thresholds [18], e.g., soda lime silica glass 70SiO$_2$ 21CaO 9Na$_2$O has an effective percolation threshold $\phi_c = 0.049\ \theta_c$, whereas the vitreous anorthite has $\phi_c = 2.25\ 10^{-5}\ \theta_c$ (Table 2).

Table 2. Percolation thresholds.

Amorphous Material	T_g, K	ϕ_c
Vitreous silica (SiO$_2$) glass	1475	0.15
Vitreous germania (GeO$_2$)	786	0.15
Soda–Lime–Silica glass (mass%): 70SiO$_2$ 21CaO 9Na$_2$O	777	7.42×10^{-4}
Vitreous B$_2$O$_3$	580	9.14×10^{-5}
Vitreous diopside (CaMgSi$_2$O$_6$)	978	6.35×10^{-7}
Vitreous anorthite (CaAl$_2$Si$_2$O$_8$)	1126	3.38×10^{-7}

An explanation was suggested in [18,19,32] that significantly lower percolation thresholds for broken bonds can be due to the structure described by the MRN model of complex oxide systems which are typically fragile. Indeed, the MRN model holds namely for complex materials that comprise network-modifying cations distributed in channels (Figure 1). Complex materials are typically fragile where Angell interpreted strong and fragile behavior of liquids in terms of differences in the topology of the configuration space potential energy hypersurfaces [59]. However, Doremus has emphasized that the implication of strong-fragile classification was that strong fluids are strongly and fragile are weakly bonded, which is misleading [60]. Examples are binary silicate glasses that are strong although they have many non-bridging oxygens. Other examples are anorthite and diopside, which have very high activation energies being quite strongly bounded but are very fragile [60]; therefore, the strength of CBL is characterized by the free Gibbs energy of configurons formation G_d or the enthalpy of formation of configurons H_d rather than the fragility ratio.

The bond lattice model of amorphous materials [38] replaces the system of strongly interacting ions by a congruent set of weakly interacting bonds; hence, we are dealing in the CBL of complex oxide systems with a porous system of contacting spheres rather that with a well compacted system of contacting spheres (Figure 6).

Topological descriptions are essential for the description of structures lacking long-range translational and orientational order; moreover, Hobbs et al. emphasized that the structural freedom required to form aperiodic networks is directly related to the connectivity, and the range of allowable structural possibilities can be enumerated using combinatorial geometry [61–63]. Thus, the diminishing values of configuron percolation thresholds

ϕ_c in complex oxide systems can be interpreted in terms of equivalent configuron size or its effective delocalization, which can be effectively much larger than the bond size. An example of such delocalization can be data obtained for the extremely fragile liquid ZrO_2 where the details of the chemical bonding explain the extremely low viscosity of the liquid, and the absence of a first sharp diffraction peak and the variety of large oxygen coordination and polyhedral connections with short Zr–O bond lifetimes, induced by the relatively large ionic radius of zirconium, disturbs the evolution of intermediate-range ordering, which leads to an increased delocalization in the ionic Zr–O bonding [64]. The higher the fragility ratio, the larger the effective configuron radius and its delocalization [32], because the liquid–glass transition occurs in fragile materials at lower percolation thresholds compared to strong liquids. The effective configuron radius, r_c, can be assessed as:

$$r_c = r_d (\theta_c / \phi_c)^{1/3}, \tag{9}$$

where r_d is the bond radius (half of bond length). Therefore, the effective volume of a configuron is given by $V_c = V_d \theta_c / \phi_c$, where V_d is the volume of an instantaneous or non-relaxed configuron, θ_c is the universal critical density in the 3D space (Scher–Zallen invariant), and ϕ_c is found by comparing the actual glass transition temperature with that given by Equation (2). Materials such as amorphous silica and germania have small effective radii configurons localized on broken bonds, and because of that, they show a smaller dependence on thermal history, which conforms with experimental findings [65]. In fragile materials, the effective configuron radii considerable exceed bond radii, $r_c \gg r_d$. For example, vitreous B_2O_3 has $r_c = 11.79 r_d$, which is due to its specific structure. Indeed, both crystalline and vitreous boron oxide consist of planar oxygen triangles centered by boron, most of which accordingly to X-ray diffraction data are arranged in boroxol rings [22]. The two-dimensional nature of the B_2O_3 network means that the third direction is added by crumbling of the planar structures in a three-dimensional amorphous boric oxide, which results in effective large-size configuron compared bond length. This results in percolation thresholds ϕ_c dependent on the geometry of involved entities and the relatively large radii of configurons which are considered spherically symmetric. Boron-containing silicate glasses are also characterized by their specific structure dependent on the boron coordination, which changes with composition [66]. Additional value can be also brought by analyzing the actual MRO structure of glasses such of the facets of clusters formed in the glass transition process analysis based on X-ray diffraction patterns [67]. There is a link between fragility and internal structural changes observed on cooling of some liquids [64,68–70]. Synchrotron X-ray scattering studies have shown an increasing degree of short- and medium-range order that develops with increased supercooling, and the analysis of the atomic and electronic structure of the alloy in liquid and glassy states revealed the formation of chemical short-range order in the temperature range corresponding to such a non-Arrhenius behavior [68]. It was demonstrated for several metallic glass-forming liquids that the rate of this structural ordering as a function of temperature correlates with the kinetic fragility of the liquid, demonstrating a structural basis for fragility [69]. Moreover, it was shown that the fragility is a sign of instability of short and medium range order in liquids with molecular dynamic simulation supporting observed structure variation [70]. Thus, the glass transition although being a kinetically controlled process [28] is nevertheless linked to structural rearrangements [31] and has thermodynamically related features and similarity to second-order thermodynamic phase transformations [71].
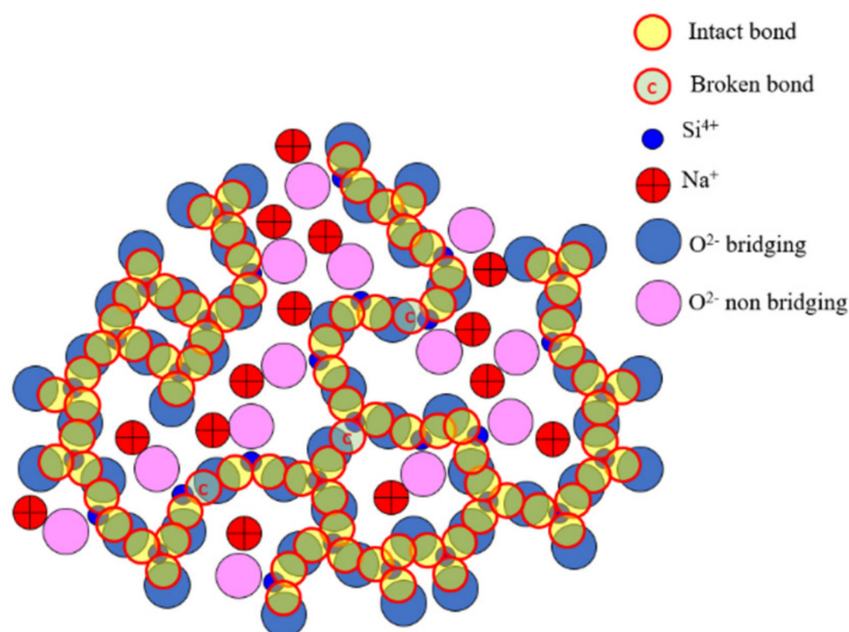
Figure 6. Schematic of congruent set of weakly interacting bonds of a sodium–silicate glass with percolation ionic channels formed by alkali cations and chains of intact Si-O-Si bonds. Three configurons are explicitly shown. Chains formed by chemical bonds resemble a system of rods and can percolate at a much lower volume fractions $\phi_c \ll \theta_c$ than the system of compacted spheres that percolate at $\phi_c = \theta_c$.

4. Conclusions

The MRN model of complex oxide glasses is confirmed by experimental techniques and computer simulations. Its utilization enables the understanding of glass properties observed such as glass mechanical and chemical durability by establishing the distribution of weakly bonded glass modifiers, ion exchange sites, hydrolysis sites, and access of water to those sites. The MRN model has also found its place in the CPT of glass transition enabling understanding of the reduced percolation threshold in complex oxide systems. Thus, the results given by the MRN model may be useful for understanding the nature and criteria of glass transition, including additional arguments to macroscopic percolation clusters observed at glass transition and theoretical interpretations of glass transition.

References

1. Greaves, G.N.; Fontaine, A.; Lagarde, P.; Raoux, D.; Gurman, S.J. Local structure of silicate glasses. *Nature* **1981**, *293*, 611–616. [CrossRef]
2. Greaves, G.N. EXAFS and the structure of glass. *J. Non-Cryst. Solids* **1985**, *71*, 203–217. [CrossRef]
3. Greaves, G.N. Structure and ionic transport in disordered silicates. *Miner. Mag.* **2000**, *64*, 441–446. [CrossRef]
4. Greaves, G.N.; Sen, S. Inorganic glasses, glass-forming liquids and amorphizing solids. *Adv. Phys.* **2007**, *56*, 1–166. [CrossRef]

5. Zachariasen, W.H. The atomic arrangement in glass. *J. Am. Chem. Soc.* **1932**, *54*, 3841–3851. [CrossRef]
6. Cormack, N.A.; Du, J.; Zeitler, R.T. Alkali ion migration mechanisms in silicate glasses probed by molecular dynamics simula-tions. *Phys. Chem. Chem. Phys.* **2002**, *4*, 3193–3197. [CrossRef]
7. Ojovan, M.I. Mass spectrometric evidencing on modified random network microstructure and medium range order in silicate glasses. *J. Non-Cryst. Solids* **2016**, *434*, 71–78. [CrossRef]
8. Donald, I.W. *Waste Immobilisation in Glass and Ceramic Based Hosts*; Wiley: Chichester, UK, 2010; 507p.
9. Greaves, G.N.; Ngai, K.L. Reconciling ionic-transport properties with atomic structure in oxide glasses. *Phys. Rev. B* **1995**, *52*, 6358–6380. [CrossRef] [PubMed]
10. Le Losq, C.; Neuville, D.R.; Chen, W.; Florian, P.; Massiot, D.; Zhou, Z.; Greaves, G.N. Percolation channels: A universal idea to describe the atomic structure and dynamics of glasses and melts. *Sci. Rep.* **2017**, *7*, 16490. [CrossRef]
11. Du, J.; Cormack, A. The medium range structure of sodium silicate glasses: A molecular dynamics simulation. *J. Non-Cryst. Solids* **2004**, *349*, 66–79. [CrossRef]
12. Gedeon, O.; Liška, M.; Macháček, J. Connectivity of Q-species in binary sodium-silicate glasses. *J. Non-Cryst. Solids* **2008**, *354*, 1133–1136. [CrossRef]
13. Nesbitt, H.; Henderson, G.; Bancroft, G.; Ho, R. Experimental evidence for Na coordination to bridging oxygen in Na-silicate glasses: Implications for spectroscopic studies and for the modified random network model. *J. Non-Cryst. Solids* **2015**, *409*, 139–148. [CrossRef]
14. Adams, S.; Swenson, J. Structure conductivity correlation in reverse Monte Carlo models of single and mixed alkali glasses. *Solid State Ion.* **2004**, *175*, 665–669. [CrossRef]
15. Jantzen, C.M.; Brown, K.G.; Pickett, J.B. Durable Glass for Thousands of Years. *Int. J. Appl. Glas. Sci.* **2010**, *1*, 38–62. [CrossRef]
16. Ojovan, M.I.; Lee, W.E. Topologically disordered systems at the glass transition. *J. Phys. Condens. Matter* **2006**, *18*, 11507–11520. [CrossRef]
17. Ozhovan, M.I. Topological characteristics of bonds in SiO2 and GeO2 oxide systems upon a glass-liquid transition. *J. Exp. Theor. Phys.* **2006**, *103*, 819–829. [CrossRef]
18. Ojovan, M.I.; Lee, W.E. Connectivity and glass transition in disordered oxide systems. *J. Non-Cryst. Solids* **2010**, *356*, 2534–2540. [CrossRef]
19. Ojovan, M.I. Ordering and structural changes at the glass–liquid transition. *J. Non-Cryst. Solids* **2013**, *382*, 79–86. [CrossRef]
20. El-Shamy, T.M. The chemical durability of K2O–CaO–MgO–SiO2 glasses. *Phys. Chem. Glas.* **1973**, *14*, 1–5.
21. Moesgaard, M.; Keding, R.; Skibsted, J.; Yue, Y. Evidence of Intermediate-Range Order Heterogeneity in Calcium Aluminosilicate Glasses. *Chem. Mater.* **2010**, *22*, 4471–4483. [CrossRef]
22. Zhang, Y.; Yang, G.; Yue, Y. Calorimetric Signature of Structural Heterogeneity in a Ternary Silicate Glass. *J. Am. Ceram. Soc.* **2013**, *96*, 3035–3037. [CrossRef]
23. Zarzycki, J. *Glasses and the Vitreous State*; Cambridge University Press: New York, NY, USA, 1982.
24. Varshneya, A.K. *Fundamentals of Inorganic Glasses*; Society of Glass Technology: Sheffield, UK, 2006.
25. Sanditov, D.S. A criterion for the glass–liquid transition. *J. Non-Cryst. Solids* **2014**, *385*, 148–152. [CrossRef]
26. Tournier, R.F. Fragile-to-fragile liquid transition at Tg and stable-glass phase nucleation rate maximum at the Kauzmann temperature TK. *Phys. B Condens. Matter* **2014**, *454*, 253–271. [CrossRef]
27. Zheng, Q.; Zhang, Y.; Montazerian, M.; Gulbiten, O.; Mauro, J.C.; Zanotto, E.D.; Yue, Y. Understanding Glass through Differential Scanning Calorimetry. *Chem. Rev.* **2019**, *119*, 7848–7939. [CrossRef] [PubMed]
28. Sanditov, D.S.; I Ojovan, M. Relaxation aspects of the liquid–glass transition. *Physics-Uspekhi* **2019**, *62*, 111–130. [CrossRef]
29. Sanditov, D.S.; Ojovan, M.I.; Darmaev, M.V. Glass transition criterion and plastic deformation of glass. *Phys. B Condens. Matter* **2020**, *582*, 411914. [CrossRef]
30. Yue, Y.-Z. Characteristic temperatures of enthalpy relaxation in glass. *J. Non-Cryst. Solids* **2008**, *354*, 1112–1118. [CrossRef]
31. Ojovan, M.I.; Louzguine-Luzgin, D.V. Revealing Structural Changes at Glass Transition via Radial Distribution Functions. *J. Phys. Chem. B* **2020**, *124*, 3186–3194. [CrossRef]
32. Ojovan, M.I. Configurons: Thermodynamic Parameters and Symmetry Changes at Glass Transition. *Entropy* **2008**, *10*, 334–364. [CrossRef]
33. Stanzione, J.F., III; Strawhecker, K.; Wool, R. Observing the twinkling fractal nature of the glass transition. *J. Non-Cryst. Solids* **2011**, *357*, 311–319. [CrossRef]
34. Albert, S.; Bauer, T.; Michl, M.; Biroli, G.; Bouchaud, J.-P.; Loidl, A.; Luckenheimer, P.; Tourbot, R.; Wiertel-Gasquet, C.; Ladieu, F. Fifth-order susceptibility unveilqs growth of thermodynamic amorphous order in glass-formers. *Science* **2016**, *352*, 1308–1311. [CrossRef]
35. Tournier, R.F. Glass phase and other multiple liquid-to-liquid transitions resulting from two-liquid phase competition. *Chem. Phys. Lett.* **2016**, *665*, 64–70. [CrossRef]
36. Tournier, R.F. First-order transitions in glasses and melts induced by solid superclusters nucleated and melted by homogeneous nucleation instead of surface melting. *Chem. Phys.* **2019**, *524*, 40–54. [CrossRef]
37. Tournier, R.F. Homogeneous nucleation of phase transformations in supercooled water. *Phys. B Condens. Matter* **2020**, *579*, 411895. [CrossRef]

38. Angell, C.A.; Rao, K.J. Configurational excitations in condensed matter and the "bond lattice". Model for the liquid-glass tran-sition. *J. Chem. Phys.* **1972**, *57*, 470–481. [CrossRef]
39. Cunningham, D.W. *Set Theory. A First Course*; Cambridge University Press: New York, NY, USA, 2016.
40. Benigni, P. Thermodynamic analysis of the classical lattice-hole model of liquids. *J. Non-Cryst. Solids* **2020**, *534*, 119942. [CrossRef]
41. Benigni, P. CALPHAD modeling of the glass transition for a pure substance, coupling thermodynamics and relaxation kinetics. *Calphad* **2021**, *72*, 102238. [CrossRef]
42. Scher, H.; Zallen, R. Critical Density in Percolation Processes. *J. Chem. Phys.* **1970**, *53*, 3759–3761. [CrossRef]
43. Isichenko, M.B. Percolation, statistical topography, and transport in random media. *Rev. Mod. Phys.* **1992**, *64*, 961–1043. [CrossRef]
44. Turnbull, D.; Cohen, M.H. On the Free-volume Model of the Liquid-glass Transition. *J. Chem. Phys.* **1970**, *52*, 3038–3041. [CrossRef]
45. Sahimi, M. *Applications of Percolation Theory*; Taylor & Francis: London, UK, 1994.
46. Hunt, A. Finite-size effects on the glass transition temperature. *Solid State Commun.* **1994**, *90*, 527–532. [CrossRef]
47. Tournier, R.F.; Ojovan, M.I. Dewetting temperatures of prefrozen and grafted layers in solid ultrathin films viewed as melt-memory effects. *Phys. B Condens. Matter* **2021**, *611*, 412796. [CrossRef]
48. Roller, J.; Laganapan, A.; Meijer, J.-M.; Fuchs, M.; Zumbusch, A. Observation of liquid glass in suspensions of ellipsoidal colloids. *Proc. Natl. Acad. Sci. USA* **2021**, *118*. [CrossRef] [PubMed]
49. Ozhovan, M.I. Dynamic uniform fractals in emulsions. *J. Exp. Theor. Phys.* **1993**, *77*, 939–943.
50. Ojovan, M.I.; Lee, W.E. Glassy wasteforms for nuclear waste immobilisation. *Metall. Mater. Trans. A* **2011**, *42*, 837–851. [CrossRef]
51. Ojovan, M.I.; Travis, K.P.; Hand, R.J. Thermodynamic parameters of bonds in glassy materials from viscosity–temperature relationships. *J. Phys. Condens. Matter* **2007**, *19*, 415107. [CrossRef] [PubMed]
52. Ojovan, M.I. On Viscous Flow in Glass-Forming Organic Liquids. *Molecules* **2020**, *25*, 4029. [CrossRef]
53. Zhao, J.; Simon, S.L.; McKenna, G.B. Using 20-million-year-old amber to test the super-Arrhenius behaviour of glass-forming systems. *Nat. Commun.* **2013**, *4*, 1783. [CrossRef]
54. McKenna, G.B.; Zhao, J. Accumulating evidence for non-diverging time-scales in glass-forming fluids. *J. Non-Cryst. Solids* **2015**, *407*, 3–13. [CrossRef]
55. Yoon, H.; McKenna, G.B. Testing the paradigm of an ideal glass transition: Dynamics of an ultrastable polymeric glass. *Sci. Adv.* **2018**, *4*, eaau5423. [CrossRef]
56. Broadbent, S.R.; Hammersley, J.M. Percolation processes I. Crystals and mazes. *Proc. Camb. Philos. Soc.* **1957**, *53*, 629–641. [CrossRef]
57. Berkowitz, B.; Ewing, R.P. Percolation Theory and Network Modeling Applications in Soil Physics. *Surv. Geophys.* **1998**, *19*, 23–72. [CrossRef]
58. Ozhovan, M.I.; Semenov, K.N. Percolation in a system of polydispersed particles. *J. Exp. Theor. Phys.* **1992**, *75*, 696–698.
59. Angell, C. Perspective on the glass transition. *J. Phys. Chem. Solids* **1988**, *49*, 863–871. [CrossRef]
60. Doremus, R.H. Viscosity of silica. *J. Appl. Phys.* **2002**, *92*, 7619–7629. [CrossRef]
61. Hobbs, L.W. Network topology in aperiodic networks. *J. Non-Cryst. Solids* **1995**, *192–193*, 79–91. [CrossRef]
62. Hobbs, L.W.; Jesurum, C.E.; Pulim, V.; Berger, B. Local topology of silica networks. *Philos. Mag. A* **1998**, *78*, 679–711. [CrossRef]
63. Hobbs, L.W.; Jesurum, C.E.; Berger, B. The topology of silica networks. In *Structure and Imperfections in Amorphous and Crystalline SiO₂*; Devine, R.A., Duraud, J.-P., Dooryhee, E., Eds.; John Wiley & Sons: London, UK, 2000.
64. Kohara, S.; Akola, J.; Patrikeev, L.; Ropo, M.; Ohara, K.; Itou, M.; Fujiwara, A.; Yahiro, J.; Okada, J.T.; Ishikawa, T.; et al. Atomic and electronic structures of an extremely fragile liquid. *Nat. Commun.* **2014**, *5*, 5892. [CrossRef]
65. Koike, A.; Tomozawa, M. Towards the origin of the memory effect in oxide glasses. *J. Non-Cryst. Solids* **2008**, *354*, 3246–3253. [CrossRef]
66. Lu, X.; Deng, L.; Du, J.; Vienna, J.D. Predicting boron coordination in multicomponent borate and borosilicate glasses using analytical models and machine learning. *J. Non-Cryst. Solids* **2021**, *553*, 120490. [CrossRef]
67. Cheng, S. New Interpretation of X-ray Diffraction Pattern of Vitreous Silica. *Ceramics* **2021**, *4*, 83–96. [CrossRef]
68. Louzguine-Luzgin, D.; Belosludov, R.; Yavari, A.R.; Georgarakis, K.; Vaughan, G.; Kawazoe, Y.; Egami, T.; Inoue, A. Structural basis for supercooled liquid fragility established by synchrotron-radiation method and computer simulation. *J. Appl. Phys.* **2011**, *110*, 043519. [CrossRef]
69. Mauro, N.A.; Blodgett, M.; Johnson, M.L.; Vogt, A.J.; Kelton, K.F. A structural signature of liquid fragility. *Nat. Commun.* **2014**, *5*, 4616. [CrossRef] [PubMed]
70. Louzguine-Luzgin, D.; Georgarakis, K.; Andrieux, J.; Hennet, L.; Morishita, T.; Nishio, K.; Belosludov, R. An atomistic study of the structural changes in a Zr–Cu–Ni–Al glass-forming liquid on vitrification monitored in-situ by X-ray diffraction and molecular dynamics simulation. *Intermetallics* **2020**, *122*, 106795. [CrossRef]
71. Ojovan, M.I. Glass formation. In *Encyclopedia of Glass Science, Technology, History, and Culture*; Richet, P., Conradt, R., Takada, A., Dyon, J., Eds.; Wiley: Hoboken, NJ, USA, 2021; pp. 249–259.